

System Identification of a 6 m² Kite Power System in Fixed-Tether Length Operation

Mostafa A. Rushdi^{1,4}, Tarek N. Dief², Amr M. Halawa², Shigeo Yoshida²

Abstract – The traction force of a kite system can be utilized for extracting energy from high-altitude wind. This paper discusses a system identification algorithm derived to obtain real-time governing equations for the kite system based on real-flight data, obtained from a 6 m² kite power system developed in Kyushu University as an airborne wind energy project. The paper presents the system set-up, the design, the experimental results, a system identification algorithm, and the parameters identified for the kite used. The current stage of the project considers the kite application as a fixed-tether length system with a ground kite control unit. The control strategy is designed to work as a hardware-in-the-loop to keep receiving the data and controlling the kite in real time. The experimental tests employed are divided into four distinct ones, and the data of the kite's attitude, position, and tension forces are recorded. The tension forces resulted from these tests are presented for different wind speeds and flight modes. Ultimately, a novel system identification algorithm that evaluates the correlation between the tension force and the kite's rolling angle over the four tests is applied, thereby enabling to study the kite behavior as a preliminary step for the achievement of autonomous flight. **Copyright © 2020 Praise Worthy Prize S.r.l. - All rights reserved.**

Keywords: Airborne Wind Energy, Kite, System Identification

Nomenclature

a_1, a_2	Numerator coefficients of the open-loop TF
b_1, b_2	Denominator coefficients of the open-loop TF
$G(z^{-1})$	Open-loop TF of the model in the z-domain
$U(z^{-1})$	System input defined as u_s in the z-domain
$Y(z^{-1})$	Estimated tension force obtained from system identification in the z-domain
Y_m	Measured tension force obtained from sensor
z^{-1}	Backward shift operator in the z-domain
AWE	Airborne Wind Energy
GPS	Global Positioning System
HAWT	Horizontal Axis Wind Turbines
HIL	Hardware-In-The-Loop
IMU	Inertial Measurement Unit
KCU	Kite Control Unit
MSE	Mean Square Error
RC	Remote Control
SI	System Identification
TF	Transfer Function

I. Introduction

Airborne Wind Energy (AWE) is an emerging renewable power technology, which utilizes tethered

flying objects, devices, or vehicles [1]-[7]. The main principle of AWE is that the flying device, a kite in this case, generates aerodynamic forces, which are transferred as tension in the tether, or effectively as mechanical energy, that could be converted to electrical energy at the ground station via a drum and a generator. So far, AWE has been demonstrated at tens of kilowatts level in a scale much smaller than what would be commercially viable in the utility sector [1], [2]. AWE systems have several advantages compared to horizontal wind turbines (HAWTs). These advantages involve the material of both the tower structure and foundations, besides the transportations, installations, and maintenance costs. As a result, AWEs can be operated with profit only in certain windy locations at heights of 50-150 meters [3]. Among the different types of AWE systems, herein kite power system, represented in Fig. 1, is studied. Many companies are following the same approach, such as Kite energy [8], KiteGen [9], and most notably Kitepower [10]. The Kitepower company is developing a 100-kW system, with a 60-m² kite's surface area. In Kyushu University, a system that is designed to capture wind energy using a tethered inflatable wing controlled by a Kite Control Unit (KCU) has been developed. Wind energy is harvested at the ground station by converting the linear motion of the tether into electric power. The current phase of this project aims to reach a height of 50 m, with a generated power of 7 kW [11]. The competitive point stems from the fact that this project is low cost but with promising results for the power generated.

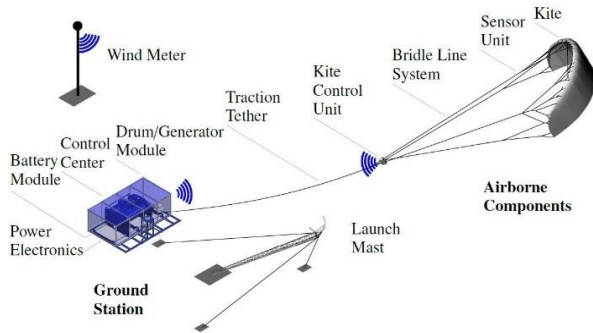


Fig. 1. Kite power system components [1]

Early work in system identification has been developed by the statistics and time-series communities. It has its roots in the work of Gauss (1809), Fisher (1912) and it is intimately related to the theory of stochastic processes. In 1960, it began to experience dramatic improvements with the start of the state-space era. Most notably the year 1965 witnessed the simultaneous appearance of two milestone seminal papers, one by Ho and Kalman [12], and the other by Aström and Bohlin [13], which gave birth to modern system identification, and established it as a new paradigm in various engineering disciplines. Since then, identification techniques and algorithms have evolved gradually and continuously [14]. Nowadays, SI techniques are used in a variety of scientific and engineering applications, including the chemical [15], medical [16], mechanical [17], aerospace [18], wind-energy [19] areas. In particular, new techniques of machine learning [20] blossomed during the past decade. By using System Identification (SI) methodology, statistical methods will be used to build a mathematical model for the dynamic system from the data measured [21]. Knowing the input and output only and treating the whole dynamical system as a black box, SI enables to come up with a transfer function that describes the system. For that reason, SI is widely used when it is hard to describe a system. In the AWE community, SI has been used in several papers, using a kite [22], [23] or an aircraft [24], [25] as a flying device. This paper presents the full prototype developed in Kyushu University including the system set-up, ground station, and the KCU. The ground station is installed on a moving truck that is used to generate wind speed at sea level that is equivalent to high-altitude wind speed. Several tests are performed to analyze the kite performance for several truck speeds and flight conditions. The tension force curves of the data obtained from the flight tests are generated and analyzed. Finally, SI algorithm that treats the whole system as a black box with one input of our choice and one output, which is obviously the tension force, is applied.

The remainder of this paper is divided into five main sections that follow the present introduction section and the earlier section on nomenclature and abbreviation. Section III presents the system components while Section IV describes the experiment that we performed. The experimental results are represented in Section V. Section

VI represents the system identification algorithm and its results. Finally, conclusions and future lines of development are reported in Section VII.

II. System Components

In Kyushu University, a 7 kW kite power system has been built which consists of a 6 m² inflatable kite wing connected with a KCU using 3 tethers; two control lines and one main tether. The other side of the KCU is connected to the ground with the main tether. The tension-meter is fixed on the ground and it is attached to the main tether. The main components of the presented system are as follows:

- *Ground station*: consists of the wireless unit and the KCU. The KCU's weight is about 3 kilograms, including the lithium battery;
- *Tether*: made of the ultra-high molecular weight polyethylen called "Dyneema," which is a light-weight ultra-strong fiber, which can withstand a maximum tension force of 2500 N;
- *Kite Control Unit*: used to steer the kite position using a servo motor. The KCU is located 12 m below the kite, and it controls the rolling motion of the kite. In the current stage of the project, there is no control on the angle of attack. The KCU has a receiver to obtain the control action for the actuator wirelessly from the RC. One end of the KCU is connected to the tension-meter in order to calculate the tension force during testing. Moreover, the data of the tension are recorded and sent in a wireless mode to the ground station. The KCU is powered by one lithium battery with an endurance of almost three hours continuous operation;
- *Measurement Unit*: fixed on the kite to record the data of position, height, and attitude. In addition, these data are sent wirelessly to the ground station with a sampling time of 0.15 second. An Arduino Microcontroller, the Global Positioning System (GPS), an inertial Measurement Unit (IMU), and pressure sensors were used to obtain these data. A compatible radio module Digi XBee has been used to send the data wirelessly to the ground station.

III. Experiment Outline

The tests have been performed using a truck, where the truck deck is considered as a ground station, holding the tension meter, which is connected to the KCU's backside with the main tether, connected to tension load sensor. In real flight tests, this tether should be longer to reach higher altitudes. The KCU's front side has been connected to the kite with 2 supplementary tethers, called control lines. The kite has been launched by hand from the border of the wind-window. After that, the figure-of-eight motion using remote control (RC) has been performed. This RC sends signals to the KCU to perform the control action, which is steering the kite right or left.

The control action is such as to yield a roll movement

of the kite, which is the only degree of freedom to be controlled. These tests have been performed in a small airport for Unmanned Aerial Vehicles (UAVs), with a runway of 750 m at Shiroshi, Saga, Japan as depicted in Figs. 2 and 3. The performed testes are summarized in Table I.

IV. Experimental Results

This section shows the experimental results obtained from the truck tests. The aim of these tests is to show the influence of changing the truck speed and flight phase on the tension force resulting from the kite. At every test, the truck should perform two complete cycles as shown in Figs. 4-9. More details for these flight tests are available in a recently published paper of the authors [11].

TABLE I
FLIGHT TESTS OUTLINE

	Test 1	Test 2	Test 3	Test 4
Speed [km/h]	40	40	50	50
Maneuver	steady	Fig.-of-8	steady	Fig.-of-8

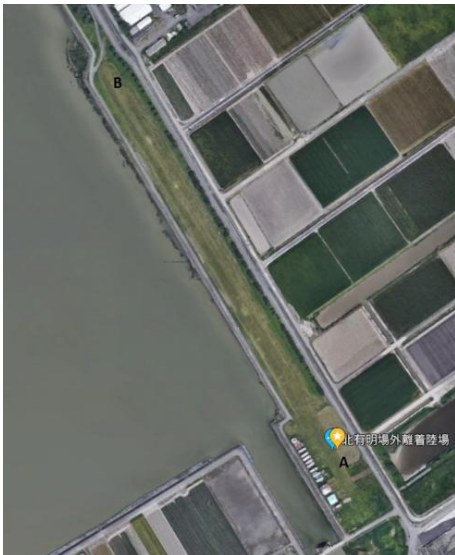


Fig. 2. Google map photo for the testing area of the kite tests, Shiroshi, Saga, Japan



Fig. 3. Truck test of the kite, with the KCU being fixed on the truck body

IV.1. Discussion of the 4 Flight Tests

IV.1.1. Test 1: Steady Flight with a Truck Speed of 40 km/h

In Test 1, it is required to obtain the tension force that resulted from the kite under some specific conditions such as the truck speed and the kite flight mode. This test has been performed for a fixed truck speed, 40 km/h, and a static ground wind speed of 1-2 m/s. The kite has been steered to fly in a steady flight mode with average pitch, roll angles of 10, and zero degrees for two complete cycles, respectively, as shown in Figs. 4 and 5. The recorded data of the tension force obtained from the kite due to its motion is depicted in Fig. 8 during the two cycles.

The average tension force was 50 N at the steady flight modes; however, it jumped to 150 N at turns due to the sudden increase in the relative wind speed. Finally, the kite has landed after 200 seconds at point A. As a result, the recorded data of the roll have a dramatic fluctuation as the kite rotates before touching the ground.

IV.1.2. Test 2: Figure-of-Eight Flight with a Truck Speed of 40 km/h

In Test 2, the truck has moved with an average speed of 40 km/h and the kite flew in a figure-of-eight path over two complete cycles as illustrated in Fig. 4. The kite has been made to flow in this particular path deliberately in order to observe the influence of this path on the measured tension force as shown in Fig. 8. The rolling angle of the kite has been fluctuating between +/- 60 degrees as shown in Fig. 5, and the pitch angle has been maintained almost constant at around 10 degrees with very small perturbations.

The average tension force obtained from the kite in Test 2 has been almost two times its value in Test 1, as the kite has been flying with different paths in the two tests, namely, a steady flight in Test 1 and a figure-of-eight flight in Test 2.

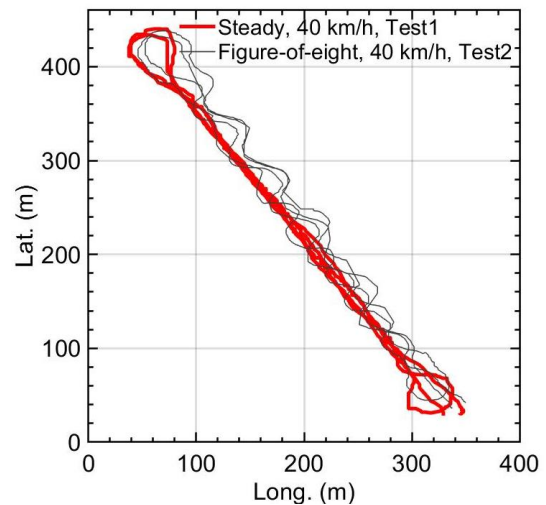


Fig. 4. Recorded data for the longitude and latitude for Tests 1 and 2

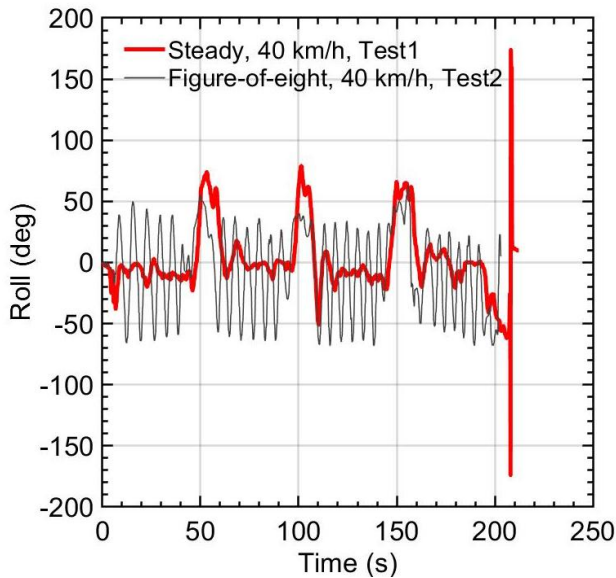


Fig. 5. Time history of the roll angle for Tests 1 and 2

IV.1.3. Test 3: Steady Flight with a Truck Speed 50 km/h

Test 3 has been performed with a truck speed of 50 km/h while the kite has been flying in a steady flight mode with average rolling and pitch angles of zero and 10 degrees, respectively. The test consists of two cycles and every one lasts for 80 seconds unlike Tests 1 and 2, which have lasted 200 seconds each. The total time to perform the two complete cycles is 160 seconds. The difference in cycle time is because of the truck speed, where the truck takes the same distance but with a higher speed as shown in Figs. 6-7. Due to the current kite motion along a straight line, the recorded tension force obtained from Test 3 is almost two times its value in Test 1. This increase has taken place as the truck speed has raised by 25 %, therefore, the relative wind speed affecting the kite increased as shown in Figs. 8 and 9.

IV.1.4. Test 4: Figure-Of-Eight Flight with Truck Speed 50km/h

The fourth test has been performed with a truck speed of 50 km/h while the kite has been flying in a figure-of-eight path as shown in Fig. 6.

The kite has been rolling with a high rate (± 60 degrees) and the pitch angle has been fluctuating at around 10 degrees as shown in Fig. 7. As expected, the average tension force for this test is the highest, because the relative wind speed has risen up due to the increase in truck speed and the movement along the figure-of-eight path. The average tension force has been between 150-200 N and sometimes it has jumped to 300-400 N, as shown in Fig. 9.

IV.2. The Effects of Flight Maneuver and Truck Speed on the Tension Forces

Figs. 8 and 9 show the impact of changing the truck

speed and the flight mode on the measured tension force obtained from the kite and recorded using the tension-meter.

In Fig. 8, a comparison between two flight modes for the same truck speed 40 km/h is presented. As shown, the steady flight generated an average tension force of 50 N, and it had very small perturbations with some ups and downs at turns. On the other hand, the tension forces of the figure-of-eight path had dramatical fluctuations that have reached 400 N with an average value of 100 N.

The tension force results, depicted in Fig. 9, have been recorded at a truck speed 50 km/h for the steady and figure-of-eight flight modes. Despite the two curves have the same behaviors as shown in Figs. 8 and 9, their average tension force for the steady flight has been 100 N and the fluctuations of the figure-of-flight have become much higher. This is because of the increase in the relative wind affecting the kite in way that allows it to get more lifting forces from the kite body.

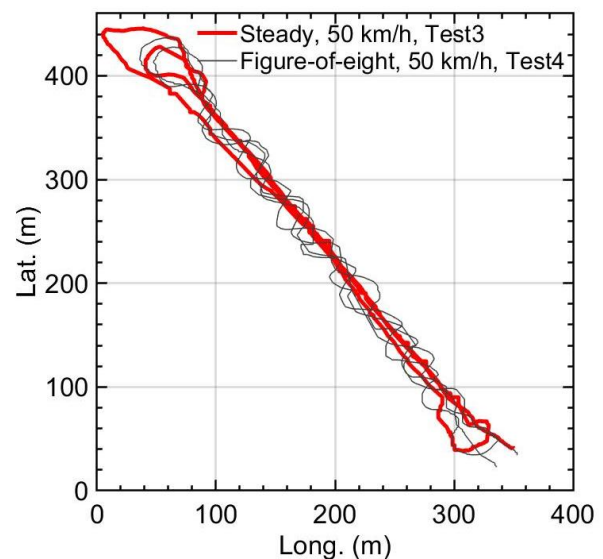


Fig. 6. Recorded data for the longitude and latitude for Tests 3 and 4

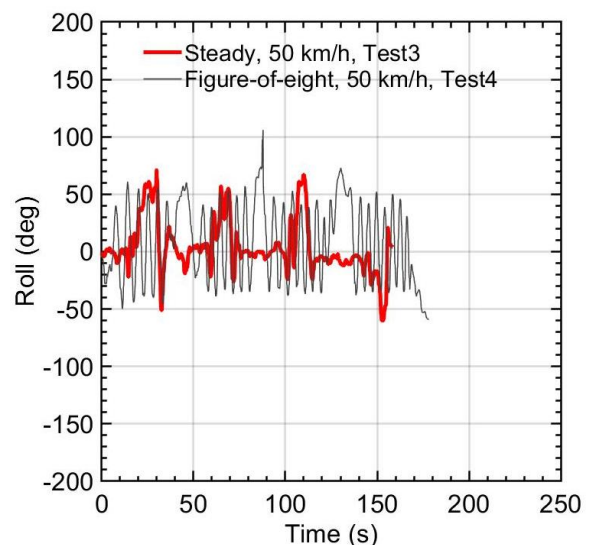


Fig. 7. Time history of the roll angle for Tests 3 and 4

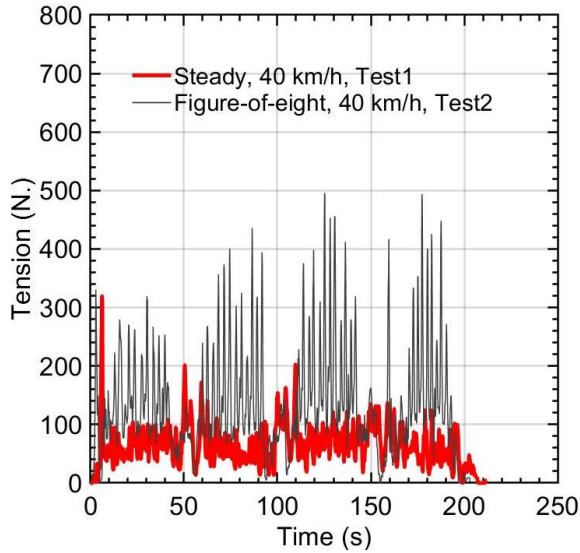


Fig. 8. Time history of the measured tension force of Test 1 and 2 at a truck speed of 40 km/h

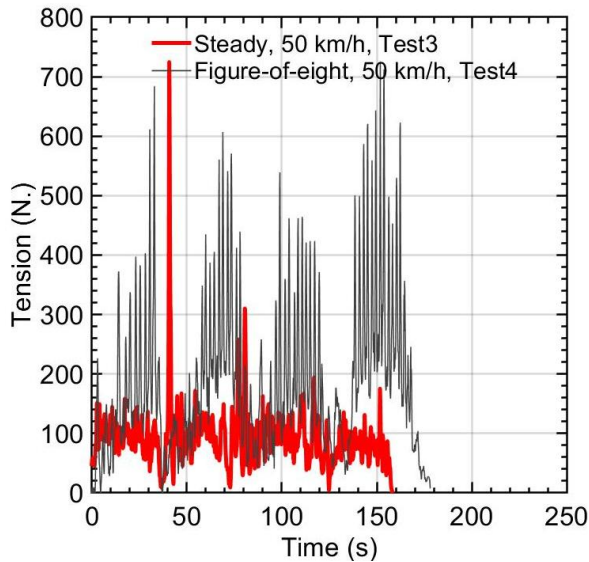


Fig. 9. Time history of the measured tension forces of Tests 3 and 4 at truck speed 50 km/h

TABLE II
AVERAGE TENSION FORCE SUMMARY

	Test 1	Test 2	Test 3	Test 4
Tension [N]	50	100	100	150

V. System Identification

The results presented in this section are based on the four flight tests illustrated in Section IV. Each one consists of two complete cycles. The flight motion of the kite is affected by different parameters, such as the change in the truck speed at turns, the steering actuation of the KCU, and the change in the kite's dynamics due to the variation of truck speed. As a result, the SI algorithm has been applied in order to identify those parameters utilizing the experimental data. The recorded data obtained from the measurement unit and the tension-

meter have been enough to identify the kite parameters a_1 , a_2 , b_1 and b_2 in real time. Since there is no exact mathematical model for the kite, the SI algorithm is the best choice to define the kite dynamics accurately. The results presented in this section will be crucial in order to develop autonomous flights in future work.

V.1. The SI Algorithm

The purpose of applying the SI algorithm is to calculate approximate values for the system parameters during flying using the recorded sensor data. Consequently, it is required to update the parameters in real time by analyzing the history of the tension force and the rolling angle [22].

There are several techniques for parameter estimation.

The one applied in this paper is the Plackett's algorithm, also known as the Recursive Least Squares (RLS) method [26]-[32].

This algorithm calculates the system parameters rapidly, without iterations. Moreover, it has no singularity and its implementation on a micro-controller is very simple. The algorithm minimizes the Mean Square Error (MSE) of the tension force measured via the tension-meter as defined by:

$$MSE = \frac{1}{k} \sum_{r=1}^k (Y_r - Y_{m,r})^2 \quad (1)$$

where k is the total number of time steps in the discrete time process, $Y_{m,r}$ is the measured data for time step r and Y_r is the estimated value determined by the SI algorithm.

The open-loop transfer function (TF) of the kite, forthcoming Eq. (5), illustrates the relation between the tension force and the kite's rolling angle. The rolling value is denoted in z-domain as U and the tension force is expressed in the same domain as Y . The block diagram of the SI algorithm is illustrated in Fig. 10. The SI algorithm estimates the tension forces and updates the coefficients of the open-loop TF a_1 , a_2 , b_1 and b_2 based on the variation of the rolling angle to generate the open-loop TF illustrated in Eq. (5). The data discussed in this section consider the tension force as a measured one.

This force data is used with the rolling angle values of the kite to calculate the estimated tension force of the four flight tests. The open-loop TF for the correlation between the tension force and the kite rolling angle in z-form can be approximated as:

$$G(z^{-1}) = \frac{Y(z^{-1})}{U(z^{-1})} = \frac{B(z^{-1})}{A(z^{-1})} \quad (2)$$

where A and B are taken as second-order polynomial equations in the z-form:

$$A(z^{-1}) = 1 + a_1 z^{-1} + a_2 z^{-2} \quad (3)$$

$$B(z^{-1}) = b_1 z^{-1} + b_2 z^{-2} \quad (4)$$

$$\frac{Y}{U}(z^{-1}) = G(z^{-1}) = \frac{b_1 z^{-1} + b_2 z^{-2}}{1 + a_1 z^{-1} + a_2 z^{-2}} \quad (5)$$

The coefficients a_1 , a_2 , b_1 and b_2 change with time due to the variation of the system's dynamics. From Eqs. (3) and (4), Eq. (2) can be written as shown in Eq. (5). This estimated tension force can be calculated by rewriting Eq. (5) in the following difference form:

$$Y_k = -a_1 Y_{k-1} - a_2 Y_{k-2} + b_1 U_{k-1} + b_2 U_{k-2} \quad (6)$$

V.2. Parameter Identification

The kite parameters are presented in this subsection, which also discusses the change occurred for every flight test. The data for the parameters a_1 and a_2 are almost constant for the four tests. By contrast, the values of b_1 and b_2 vary depending on the truck speed and the flight mode. In Test 1, the values of the parameters b_1 and b_2 have been changing at every half cycle as the truck performs the half cycle every 50 second. The values of the variables a_1 , a_2 have been -1.5, 0.5 and the variables b_1 and b_2 have been fluctuating with average values -40 and 40 respectively, as shown in Fig. 11. Test 2 had a different performance for the parameters b_1 and b_2 since the kite has been performing a figure-of-eight motion with the same truck speed 40 km/h. These parameters have started with high values since they had a very strong sudden tension force, which has affected the calculations of the SI algorithm. The average values of the parameters a_1 , a_2 , b_1 , b_2 are -1.5, 0.5, 0.5, and -0.5 respectively, as shown in Fig. 12. The third test has been performed for the truck speed 50 km/h and steady flight mode. The identified parameters of the kite a_1 and a_2 had the same values as Tests 1 and 2. However, these parameters have started with different values then settled with values -1.5 and 0.5 at a time of 40 second until the end of the two cycles. The parameters of b_1 and b_2 have been perturbing with high rate in the beginning of the simulation then became steady after 10 seconds, as shown in Fig. 13. The reason of this fluctuation is that when the initial conditions have not been close to the

exact solution, then the values have taken more time to settle. The average value for the parameters b_1 and b_2 has been zero. In Test 4, the kite has been flying in a figure-of-eight path with a truck speed of 50 km/h. The values of parameters a_1 and a_2 have been the same as in the previous three tests. The variables b_1 and b_2 have started with fluctuations then settled in a steady line with a smooth deviation with time with average values 30 and -30, as shown in Fig. 14.

V.3. Discussion

The kite power systems have several challenges, which can be summarized as follows: (a) the kite consists of a flexible membrane wing and its shape changes based on the aerodynamic force distribution and the structural design. (b) The relative wind speed affecting the kite varies along the flight path, and an accurate governing equation for the different wind speeds can be derived. (c)

There is no accurate prediction for the wind field to calculate the aerodynamic force distribution on the kite surface.

The above challenges have been addressed by applying Plackett's algorithm, which is a non-iterative SI algorithm. This paper proposes to use this algorithm to predict the kite parameters in order to obtain the dynamic model in a real time setting. Moreover, this algorithm can calculate the parameters of the system with high accuracy with no singularity. The SI technique has been implemented and applied for the four tests in order to derive the real-time governing equations as shown in Figs. 11-14. Due to the variation of the truck speeds and the flight modes, clear differences have been found in the kite dynamics over the four tests. The used SI technique needs some time to settle its parameters. Therefore, it has been noticed that the parameters are not settled for the same condition before 40 seconds of the starting time of recording. The SI technique is very powerful when trying to identify a system based on one input/output, just like our case. If there are more features that affect the output, then Machine learning techniques will be better to describe the system.

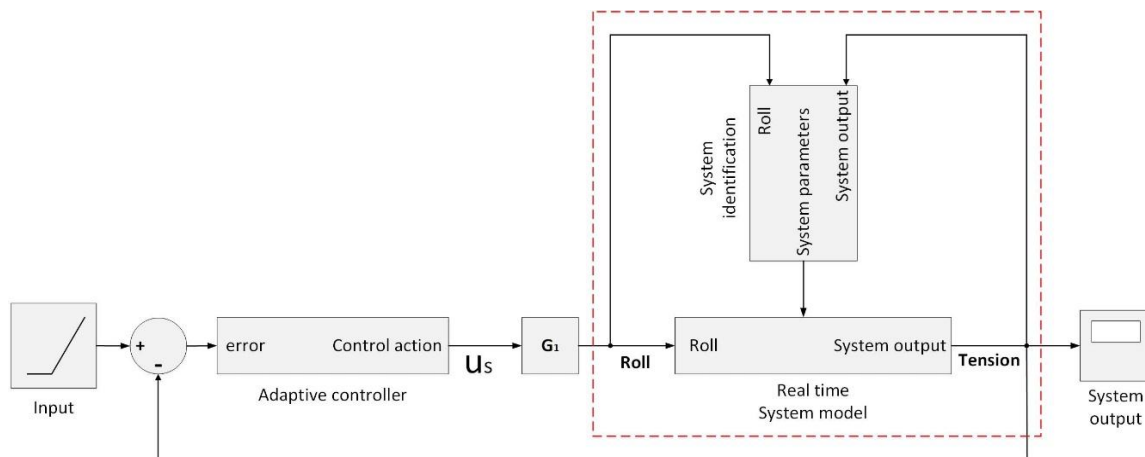


Fig. 10. Block diagram of the SI algorithm and the adaptive control system

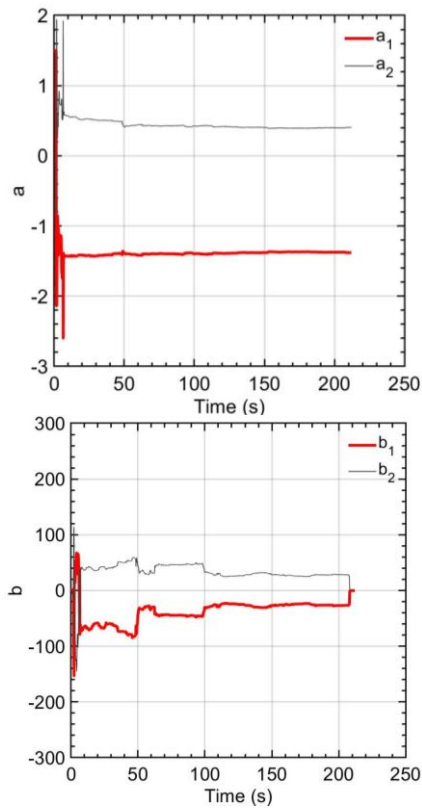


Fig. 11. Time history for the SI parameters (a and b) from Test 1

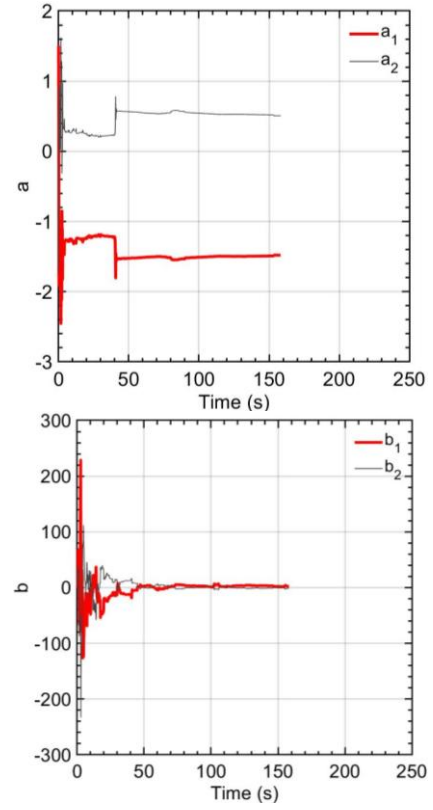


Fig. 13. Time history for the SI parameters (a and b) from Test 3

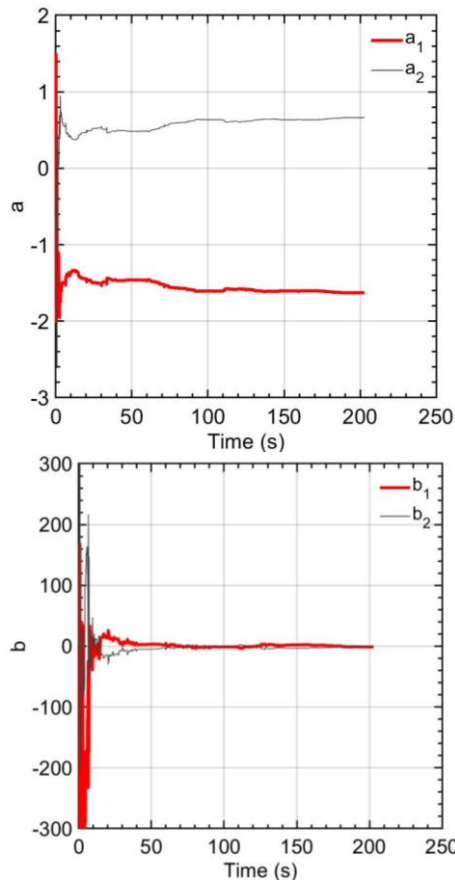


Fig. 12. Time history for the SI parameters (a and b) from Test 2

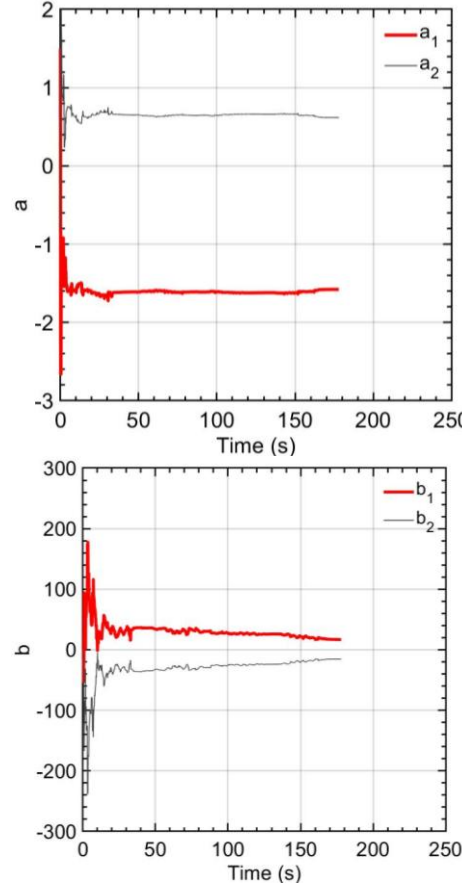


Fig. 14. Time history for the SI parameters (a and b) from Test 4

TABLE III
SI PARAMETERS SUMMARY OF THE FOUR TESTS

	Test 1	Test 2	Test 3	Test 4
a_1	-1.5	-1.5	-1.5	-1.5
a_2	0.5	0.5	0.5	0.5
b_1	-40	0.5	0.001	30
b_2	40	-0.5	-0.001	-30

VI. Conclusion

In this paper, the experimental results obtained from fixed-tether length kite operation have been presented.

This work shows the influence of increasing the wind speed and flying in different flight modes on the lifting force obtained from the kite during flying. For the same wind speed, the 6 m² kite can get an average tension force during flying in the figure-of-eight path that is almost two times its value in steady flight. Furthermore, the tension force obtained from the kite doubles its value after increasing the wind speed just 25 % of its original value for the same flight path. Four different flight tests have been performed in order to identify the relation between the tension force and the rolling angle using an SI algorithm. This technique has been assessed based on the four flight tests that have been characterized by different wind speeds and flight paths. Therefore, every test had a different correlation between the tension force and the rolling angle. Those correlations have included four parameters to define the TF that can be used to design and implement the autonomous flight. The aim of this study is to identify the kite using SI parameters in real-time. Therefore, it has been possible to apply and implement any control technique, the Model Predictive Controller (MPC) for example, in order to stabilize the kite in a real-time flight.

References

- [1] R. Schmehl, *Airborne Wind Energy: Advances in Technology Development and Research*, first ed. (Springer, Singapore, 2018).
- [2] U. Ahrens, M. Diehl, and R. Schmehl, *Airborne Wind Energy*, first ed. (Springer Science & Business Media, Berlin, 2013).
- [3] A. Cherubini, et al. Airborne Wind Energy Systems: A Review of the Technologies, *Renewable and Sustainable Energy Reviews*, 51 (2015), 1461-1476.
- [4] A. K. S. Mendonça, et al., Comparing Patent and Scientific Literature in Airborne Wind Energy, *Sustainability* 9, 915 (2017), 1-22.
- [5] M. Rushdi, S. Yoshida, and T. N. Dief, Simulation of a Tether of a Kite Power System Using a Lumped Mass Model, *IEICES Proceedings*, 42-47 (2018).
- [6] M. Rushdi, et al., Simulation of the Transition Phase for an Optimally-Controlled Tethered VTOL Rigid Aircraft for Airborne Wind Energy Generation, *AIAA Scitech 2020 Forum*. (2020), 1243.
- [7] M. N., Noom, *Theoretical analysis of mechanical power generation by pumping cycle kite power systems*, Ms.c. Dissertation, Dept. Wind Energy, TU Delft, Delft, (2013).
- [8] Kite Energy Company, [Accessed February 2020]. <http://www.kitenergy.net/>
- [9] KiteGen Company, [Accessed February 2020]. <http://www.kitegen.com/en/>
- [10] Kitepower Company, [Accessed February 2020]. <https://kitepower.nl/>
- [11] T. N. Dief, et al., Hardware-in-the-Loop (HIL) and Experimental Findings for the 7 kW Pumping Kite Power System, *AIAA Scitech 2020 Forum* (2020), 1244.
- [12] B. L. Ho and R. E. Kálmán. Effective construction of linear state-variable models from input/output functions. *at-Automatisierungstechnik* 14.1-12 (1966): 545-548.
- [13] K.-J. Åström and B. Torsten. Numerical identification of linear dynamic systems from normal operating records. *IFAC Proceedings Volumes* 2,2 (1965), 96-111.
- [14] M. Deistler. System identification and time series analysis: Past, present, and future. *Stochastic Theory and Control*. Springer, Berlin, Heidelberg, (2002), 97-109.
- [15] L. A. H. Petersen, et al., Modeling and system identification of an unconventional bioreactor used for single cell protein production. *Chemical Engineering Journal* 390 (2020): 124438.
- [16] K. K. Wallinger, and M. Huemer. Volatility Clustering in Medical Ultrasound Imaging and System Identification Based Deconvolution. *2019 IEEE International Ultrasonics Symposium (IUS)*. (2019), 1459-1462.
- [17] R. T. Torres, and F. Sergii. Brushless Direct Current Propulsion System Identification. *Integrated Computer Technologies in Mechanical Engineering*. Springer, Cham, (2020), 105-113.
- [18] M. S. Gandhi, et al. Practical system identification for small VTOL unmanned aerial vehicle. *AIAA Scitech 2019 forum*. (2019), 1982.
- [19] OQatamin, R., Mohamed, O., Abu Elhaja, W., Prediction of Power Output of Wind Turbines Using System Identification Techniques, (2020) *International Review on Modelling and Simulations (IREMOS)*, 13 (1), pp. 43-51. doi: <https://doi.org/10.15866/iremos.v13i1.17713>
- [20] T. Weber, et al. Machine Learning based System Identification Tool for data-based Energy and Resource Modeling and Simulation. *Procedia CIRP* 80 (2019), 683-688.
- [21] G. C. Clifford, and R. L. Payne. *Dynamic System Identification. Experiment Design and Data Analysis*. (Academic Press, New York, 1977).
- [22] T. N. Dief, et al., Adaptive Flight Path Control of Airborne Wind Energy Systems, *Energies*, 13, 667 (2020), 1-28.
- [23] T. N. Dief, et al., System Identification, Fuzzy Control and Simulation of a Kite Power System with Fixed Tether Length. *Wind Energy Science* 3, 1 (2018), 275-291.
- [24] G. Licitra, et al., System Identification of a Rigid Wing Airborne Wind Energy System, *arXiv preprint arXiv:1711.10010* (2017).
- [25] G. Licitra, et al., Performance Assessment of a Rigid Wing Airborne Wind Energy Pumping System, *Energy* 173 (2019), 569-585.
- [26] Dief, T., Kamra, M., Yoshida, S., Modeling, System Identification and PID-A Controller for Tethered Unmanned Quad-Rotor Helicopter, (2017) *International Review of Aerospace Engineering (IREASE)*, 10 (4), pp. 215-223. doi: <https://doi.org/10.15866/irease.v10i4.12589>
- [27] K. Dutton, *The Art of Control Engineering*. (Addison-Wesley Longman Publishing Co., Harlow, (1997).
- [28] Solo, V. The convergence of AML. *IEEE Transactions on Automatic Control*, 24, 6, (1979), 958-962.
- [29] Lockwood, S., Haase, F., & Ford, D. G. Active vibration control of machine tool structures-Part 1: DSP algorithms. *WIT Transactions on Engineering Sciences*, 44. (2003), 441-450.
- [30] Khaddaj Mallat, N., Zia, M., Mirza, N., Comparison of RLS and LMS Algorithms for Interference Cancellation in a Fixed Point to Point Microwave Link, (2017) *International Journal on Communications Antenna and Propagation (IRECAP)*, 7 (5), pp. 448-456. doi: <https://doi.org/10.15866/irecap.v7i5.12802>
- [31] Celeita Rodriguez, D., Ramos, G., Sakis Meliopoulos, A., Transmission Line Protective Relay Based on Recursive Least-Square Filters and Weights Analysis, (2018) *International Review on Modelling and Simulations (IREMOS)*, 11 (5), pp. 277-287. doi: <https://doi.org/10.15866/iremos.v11i5.14872>
- [32] Alkurawy, L., Saleh, M., Fatah, I., Saleh, A., Modeling and Identification of Human Heart System, (2019) *International Journal on Engineering Applications (IREA)*, 7 (4), pp. 130-136. doi: <https://doi.org/10.15866/irea.v7i4.17807>

Authors' information

¹IGSES, ESST, Kyushu University, Fukuoka, Japan.

²RIAM, Kyushu University, Fukuoka, Japan.

⁴Faculty of Engineering and Technology, Future University in Egypt (FUE), New Cairo, Egypt.



Mostafa A. Rushdi, Ph.D. candidate, Kyushu University, BSc, and MSc in (Aerospace Engineering, Cairo University). Instructor in Mechanical Engineering, Future University (FUE).
Research Areas: System Dynamics, Optimization, and AI (ML-DL).

E-mails: rushdimostafa@riam.kyushu-u.ac.jp,
Mostafa.Roshdi@fue.edu.eg



Tarek N. Dief, Postdoctoral Fellow, Research Institute for Applied Mechanics (RIAM), Kyushu University, Fukuoka, Japan. BSc, and MSc (in Aerospace Engineering, Cairo University). PhD (in System Dynamic, Kyushu University).
Research Areas: AWE / Robotics/ System Dynamics.

E-mail: Tarek.na3em@riam.kyushu-u.ac.jp



Amr M. Halawa, Postdoctoral Researcher, Research Institute for Applied Mechanics, Kyushu University, Fukuoka, Japan. BSc, and MSc (in Aerospace Engineering, Cairo University). PhD (in Wind Energy, Kyushu University).

Research Areas: Wind Energy / CFD / UAVs / Flow Control.

E-mail: amrhalawa@kyudai.jp



Dr. Engineer **Shigeo Yoshida**, Professor, Research Institute for Applied Mechanics, Kasuga, Fukuoka, Japan Research Area: Wind Energy.

E-mail: yoshidas@riam.kyushu-u.ac.jp